

How ripples turn into dots: modeling ion-beam erosion under oblique incidence

Sebastian Vogel and Stefan J. Linz

Institut für Theoretische Physik, Universität Münster,

Wilhelm-Klemm-Str.9, 48149 Münster, Germany

(Dated: November 11, 2018)

Abstract

Pattern formation on semiconductor surfaces induced by low energetic ion-beam erosion under normal and oblique incidence is theoretically investigated using a continuum model in form of a stochastic, nonlocal, anisotropic Kuramoto-Sivashinsky equation. Depending on the size of the parameters this model exhibits hexagonally ordered dot, ripple, less regular and even rather smooth patterns. We investigate the transitional behavior between such states and suggest how transitions can be experimentally detected.

PACS numbers: 68.55.-a, 79.20.-m, 02.60.Lj

Self-organized structure formation on the nanoscale induced by ion-beam erosion, i.e. the removal of target material by bombarding its surface with ionized particles, has recently turned into a highly active research area of surface science with deep connections to the modern theory of non-equilibrium systems. Since the work of Navez et al. [1] in 1962 it is known that, under *oblique incidence* of the ions, often washboard-like *ripple* patterns oriented normally to the beam direction can be observed on the surface (for recent reviews cf. [2, 3]). For *normal incidence* of the ions, however, just a sort of rough, unstructured surface evolution had been expected. So, it came as a surprise when Facsko et al. [4] observed quite regularly ordered, hexagonally arranged *dot* structures for semiconducting GaSb under *normal incidence* of low energetic Ar⁺-ions. Parallel to that, Frost et al. [5] found for rotated InP, InAs, InSb and GaSb targets under oblique ion incidence a variety of distinct patterns such as dot or square structures and even rather flat or smooth surfaces. Rather recently, experiments under *oblique incidence without target rotation* have revealed an even more puzzling picture. Using Si targets and ion energies $\leq 2000\text{eV}$, Ziberi et al. [6] experimentally detected transitions from ripples oriented normally to the beam direction to rather smooth surfaces by increasing the incidence angle. Similar results have also been obtained by Ziberi et al. [7], for Ge and Si targets, where in the latter case almost perfectly straight ripples have been identified. Finally using GaSb targets and low ion fluxes, Allmers et al. [8] identified a transition from hexagonal dot patterns to ripples oriented tangentially to the beam direction for small off-normal incidence.

The theoretical understanding of the hexagonally ordered dot structures under *normal incidence* has posed a particular challenge because the standard continuum model for the evolution of the morphology $H(\mathbf{x}, t)$ for ion-beam erosion, the anisotropic Kuramoto-Sivashinky equation (aKSE)[3, 9, 10] does not seem to reproduce such patterns in its isotropic limit (iKSE), $\partial_t H = F_0 + a_1 \nabla^2 H + a_2 \nabla^4 H + a_3 (\nabla H)^2 + \eta$. Therefore, two distinct generalizations of the iKSE have been put forward: Using different physical reasoning, Kim et al. [12] and Castro et al. [13] have suggested the inclusion of a term proportional to $\nabla^2 (\nabla H)^2$. Although this extended KSE (already studied in the context of amorphous surface growth [14]) might show patterns resembling hexagonally short-range ordered dots for some parameter values [13], it typically exhibits an irregular cellular pattern with remedies of a hexagonal arrangement [14]. As an alternative to explain the hexagonally ordered dots, Facsko et al. [15] suggested the inclusion of a damping term bH with $b < 0$ in the iKSE that is known to

lead to hexagonal structures. This term, physically interpreted as the effect of redeposition of sputtered particles, fails to fulfill the fundamental symmetry of translation invariance in erosion direction $H \rightarrow H + z$ with $z = \text{constant}$. To fix that, Facsko et al. suggested to replace bH by $b(H - \overline{H})$ with \overline{H} being the spatial average over some sample area. Interpreting \overline{H} as the spatial average over the whole sample, we showed in [16] that such a non-local iKSE can be rigorously rewritten as a (local) damped iKSE (idKSE) by means of a temporally nonlocal transformation and, therefore, put the applicability of the idKSE on solid theoretical grounds.

As a consequence of [15, 16], several important questions arise: (i) How does a minimal model for ion-beam erosion under normal *and* oblique angle of incidence look like and what are its eminent emergent patterns? (ii) How does the transition from dots to ripples with varying angle of inclination happen? Is it a gradual change or a bifurcation? Does it occur at a zero or non-zero angle of incidence? (iii) How do experimentally observed smooth patterns with very low surface roughness fit in such a description? (iv) How do generic transitions between distinct patterns as function of the angle of incidence look like? In this letter, we theoretically investigate these questions on the basis of an anisotropically generalized version of a nonlocal KS equation and its damped counterpart.

Model equation. - Generalizing the recipe in [16], the balance equation for the evolution of the height function $H(x, y, t)$, $\partial_t H = \nabla \cdot \mathbf{J}_H + F + \eta$, is determined by (i) relaxational currents caused by surface diffusion and assumed to be dominantly isotropic modeled by $\nabla \cdot \mathbf{J}_H = a_2 \nabla^4 H$ with $a_2 < 0$ and (ii) and detachment contributions $F = F[\partial_x H, \partial_y H, H - \overline{H}]$ that depend on partial derivatives of H , $H - \overline{H}$ and all admissible combinations of them. Possible anisotropies stemming from ion-induced surface diffusion are at this stage neglected. Orienting the coordinate system such that the tangential component of the incoming ion flux is parallel to the x -axis, any term depending on odd order derivatives with respect to y is excluded due to the reflectional invariance along the x -axis. Expanding F in its arguments and keeping solely lowest order terms yields

$$\begin{aligned} \partial_t H = & F_0 + b(H - \overline{H}) + a_0 \partial_x H + (a_{1x} \partial_x^2 + a_{1y} \partial_y^2) H + \\ & + a_2 \nabla^4 H + a_{3x} (\partial_x H)^2 + a_{3y} (\partial_y H)^2 + \eta. \end{aligned} \quad (1)$$

The physical significance of the terms on the rhs of (1) are constant erosion velocity F_0 if all other terms on the rhs were zero, surface drift due to oblique incidence (a_0 -term),

redeposition (b -term), anisotropic surface roughening via Bradley-Harper mechanism [11] (a_{1x}, a_{1y} terms), isotropic thermal surface diffusion (a_2 -term), anisotropic tilt-dependent sputter yield (a_{3x}, a_{3y} terms) and isotropic stochasticity in the erosion process with Gaussian white noise $\eta(x, y, t)$ of covariance $2D$.

Next we simplify (1). First, the drift term $a_0\partial_x H$ in (1) is eliminated via the transformation $H(x, y, t) \rightarrow H(x - a_0t, y, t)$ implying a motion of the resulting pattern with a constant speed $-a_0$ in the x direction without any change of shape of the morphology of H . Second, (1) is recast to a local field equation via the temporally nonlocal transformation [16]

$$h = H - \overline{H} + (F_0/b)(1 - e^{bt}) + e^{bt} \int_0^{t'} \partial_t \overline{H} e^{-bt'} dt' \quad (2)$$

yielding

$$\partial_t h = bh + (a_{1x}\partial_x^2 + a_{1y}\partial_y^2)h + a_2\nabla^4 h + a_{3x}(\partial_x h)^2 + a_{3y}(\partial_y h)^2 + \eta. \quad (3)$$

Third, rescaling the time by $-(a_{1x}^2/a_2)t \rightarrow t$, length scales by $\sqrt{a_{1x}/a_2}\mathbf{x} \rightarrow \mathbf{x}$, height by $-(a_{3x}/a_{1x})h \rightarrow h$ and noise by $(a_2 a_{3x}/a_{1x}^3)\eta \rightarrow \eta$ and introducing the three coefficients $\gamma = (a_2/a_{1x}^2)b > 0$, $\alpha = a_{1y}/a_{1x}$, $\beta = a_{3y}/a_{3x}$, leads to

$$\partial_t h = -(\gamma + \partial_x^2 + \alpha \partial_y^2 + \nabla^4)h + (\partial_x h)^2 + \beta(\partial_y h)^2 + \eta. \quad (4)$$

The anisotropic, damped KS equation (adKSE) (4) constitutes our minimal model for erosion under normal and oblique incidence. The parameters α and β measure the relative anisotropies of the surface roughening and the sputter yield whereas the third parameter $\gamma \geq 0$ the rescaled damping. The limit $\gamma = 0$ is the aKSE [3, 9, 10], whereas the limit $\alpha = 1 = \beta$ yields the idKSE [15, 16].

Two properties of Eq.(4) are of subsequent interest. (A) The parameter range $\alpha > 1$ can be mapped to the range $0 < \alpha < 1$ and vice versa by flipping the coordinate system, i.e. $x \rightarrow y$, $y \rightarrow x$ and rescaling time by $\alpha^2 t \rightarrow t$, length scales by $\sqrt{\alpha}\mathbf{x} \rightarrow \mathbf{x}$, height by $(\beta/\alpha)h \rightarrow h$ and the noise by $(\beta/\alpha^3)\eta \rightarrow \eta$ and transforming the coefficients, $\tilde{\gamma} = \gamma/\alpha^2$, $\tilde{\alpha} = 1/\alpha$ and $\tilde{\beta} = 1/\beta$. This yields the functionally equivalent form $\partial_t h = -(\tilde{\gamma} + \partial_x^2 + \tilde{\alpha} \partial_y^2 + \nabla^4)h + (\partial_x h)^2 + \tilde{\beta}(\partial_y h)^2 + \eta$. Consequently, the parameter sets (γ, α, β) with $\alpha < 1$ and $(\gamma/\alpha^2, 1/\alpha, 1/\beta)$ with $1/\alpha = \tilde{\alpha} \geq 1$ lead to the same dynamics. (B) The unscaled version of Eq.(4), i.e. Eq.(3), possesses the invariance under the combined transformation $h \rightarrow -h$, $a_{3x} \rightarrow -a_{3x}$, $a_{3y} \rightarrow -a_{3y}$. This implies that the corresponding morphologies are reflected about $h = 0$ if the signs of a_{3x} and a_{3y} are inverted, and, consequently, the role of mounds and valleys of the surface profile are

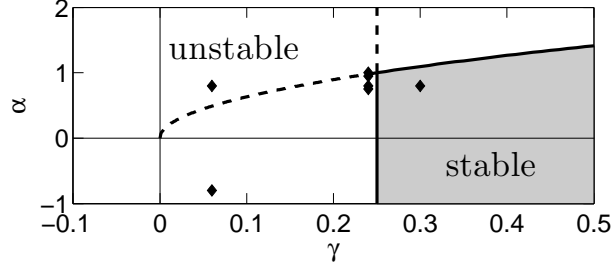


FIG. 1: Stability diagram of the flat front solution $h_{FF} = 0$ for $\eta = 0$. Markers indicate parameter values for subsequently used plots of the morphology.

exchanged. In Eq.(4) this invariance is hidden in the scaling.

Since the coefficients in (1) depend on the angle of incidence and various other parameters such as ion flux and type, target material etc. and are not well known, we subsequently study how the properties of (4) parametrically depend on the anisotropies and the damping without reference to a specific material and, by that, explore the pattern forming properties of Eq.(4).

Onset of pattern formation. - The non-stochastic limit of (4) obviously possesses a flat front solution $h_{FF} = h(\mathbf{x}, t) = 0$ corresponding to $H_{FF} = F_0 t$ as primary pattern. Its linear stability, determined by the growth or decay of small superimposed perturbations $h(\mathbf{x}, t) \propto \exp(i\mathbf{k} \cdot \mathbf{x} + \sigma t)$ in the linearized version of (4) yields the growth rate $\sigma(\mathbf{k}) = -\gamma + k_x^2 + \alpha k_y^2 - \mathbf{k}^4$ as function of the wave-number $\mathbf{k} = (k_x, k_y)$. The corresponding critical wave numbers are determined by (i) $k_x = 0$ and $k_y = \sqrt{\alpha/2}$ or (ii) $k_x = \sqrt{1/2}$ and $k_y = 0$. Consequently, $h(\mathbf{x}, t) = 0$ is linearly unstable (i) with respect to plane wave perturbations in y -direction if $\gamma < \alpha^2/4$ and $\alpha \geq 1$ or (ii) with respect to plane wave perturbations in x -direction if $\gamma < 1/4$ and $\alpha \leq 1$. In Fig. 1 the results of the linear stability analysis of $h_{FF} = 0$ are shown. Note the significant difference to the aKSE corresponding to the vertical line at $\gamma = 0$ where for $a_{1x} < 0$ and/or $a_{1y} < 0$ no stable flat front solutions can be obtained. Similar arguments also apply to any nonlinear extension of the aKSE.

Instability of perfect ripples. - Assuming $\eta = 0$ and a perfect ripple state $h_n(x, y, t) = h_n(x, t)$ normal to the incidence direction (n -ripples) obeying $\partial_t h_n = -(\gamma + \partial_x^2 + \partial_x^4)h_n + (\partial_x h_n)^2$, the evolution of a slightly perturbed height function $h(x, y, t) = h_n(x, t) + p(y, t)$ in y -direction is governed by $\partial_t p = -(\gamma + \alpha \partial_y^2 + \partial_y^4)p + \beta (\partial_y p)^2$. Linearizing and inserting periodic perturbations $p = e^{ik_y y + \tilde{\sigma} t}$ yields the maximum growth rate $\tilde{\sigma}_{max} = -\gamma + \alpha^2/4$ implying that

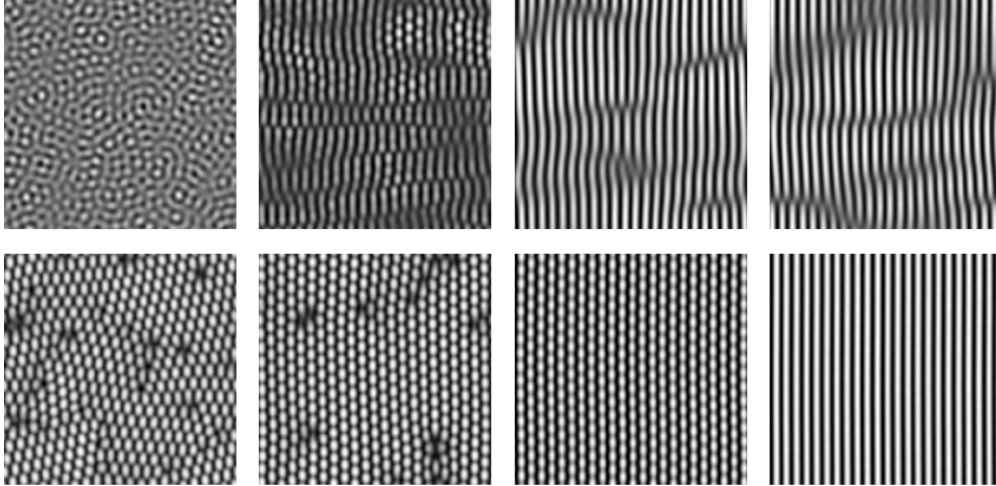


FIG. 2: Snapshot of the surface morphologies for $\gamma = 0.24$, $\beta = 2.0$ each and $\alpha = 1.0, 0.95, 0.8, 0.75$ (from left to right). Upper row: early stages at $t = 200, 620, 400, 400$ (from left to right). Lower row: later stages at $t = 10^4$ each.

n-ripple patterns are unstable against p -perturbation for $\gamma < \alpha^2/4$ with a critical wave number $\tilde{k} = \sqrt{\alpha/2}$. Similarly, a perfect ripple state $h_t(x, y, t) = h_t(y, t)$ tangential to the incidence direction (t -ripples) is unstable with respect to a slight perturbation $p(x, t)$ in x -direction for $\gamma < 1/4$ with a critical wave number $\tilde{k} = \sqrt{1/2}$. Consequently, such perfect t - or n -ripple patterns are always unstable in the aKSE. In the adKSE, however, they are, at least for these specific types of perturbations, stable in some parameter ranges. Since Ziberi et al. [7] were able to experimentally produce basically perfectly straight ripples, the necessity of the damping term in our model equation seems to stringent.

Transition from ripples to dots. - To numerically investigate how hexagonally arranged dot patterns can turn into ripples, we fix the anisotropy of the nonlinear term in (4) to a representative value $\beta = 2$ and the damping γ to a value in the unstable regime of $h_{FF} = 0$ but close to the instability, $\gamma = 0.24$, and focus on $\alpha \leq 1$. Numerical simulations have been performed using a finite difference method with periodic boundary conditions, a mesh size 200×200 , spatial step size $dx = 1$, temporal step size $dt = 0.01$, an initially flat surface and an amplitude of the Gaussian white noise $A = 5 \times 10^{-4}$ corresponding to a noise covariance $D = 4.1\bar{6} \times 10^{-6}$. Varying the anisotropy α off from its isotropic limit $\alpha = 1$ in simulations of (4), the following scenario as shown in Fig. 2 can be observed: (i) for $\alpha = 1$ the initially stochastically rough surface first evolves into a worm-like structures that turn

at later stages in a hexagonally arranged pattern with some defects. (ii) Lowering α to a value of 0.95, there is a drastic change in the preliminary stage of the evolution; slightly deformed n-ripples with some superimposed deformation structure in the y -direction occur. At later stages, however, the pattern stabilizes into a rather regular hexagonally arranged structure with even fewer defects than in (i). Consequently, even *for $\alpha \neq 1$ and $\beta \neq 1$ hexagonally arranged dot patterns can be observed*. Note, however, that these structures are not perfectly hexagonal since, as a result of any anisotropy, the amplitudes of the hexagonal dots are no longer identical. (iii) Lowering α further to a value of 0.8, the preliminary stages are n-ripples with only minor modulations; surprisingly, the later stages consist of a highly regular arrangement of dots, by far more pronounced than in the case (i) or (ii). In our simulations, the evolution to the dot structure occurs via a successive periodic lacing up of the original n-ripples in the y -direction until a basically hexagonally arranged structure being slightly elongated in the y -direction is reached. (iv) Lowering α to a value of 0.75, the preliminary stages consisting of slightly modulated n-ripples stabilize for later stages to a basically perfect n-ripple state implying that a transition from long-time dot patterns to long-time ripple patterns occurs in the range $0.78 < \alpha < 0.8$.

To investigate this transition quantitatively, we found that the temporal evolution of the surface roughness, $w(t) = \overline{\langle (h - \bar{h})^2 \rangle}^{1/2}$ with the overbar and $\langle \dots \rangle$ denoting the spatial and ensemble average, shows that the cases (ii) and (iii) are quite distinct from the other two cases. This is because $w(t)$ exhibits a double plateau behavior reflecting the transient ripple and the long-time dot structures with a turning point between these plateaus, as shown in the left panel of Fig. 3. Therefore, this turning point can be considered as an indicator for the evolution to long-time dot structures; its temporal position increases with lowering α until it vanishes at infinity. To substantiate this, we study the dependence of this turning point t_c , depicted by lozenges in the right part of Fig. 3, as function of α . Also marked are the regions where preliminary states distinct from almost perfect ripples occur. As can be read off from this figure, these preliminary states generically develop into n-ripple structures followed subsequently by a transition to long-time dot structures if $\alpha < 0.93$. For values of α smaller than about 0.78 only n-ripple structures are observable. This signals a bifurcation between long-time ripples and long-time dot structures at that value of α . To elucidate these results, this transition is not just restricted to the close vicinity of normal to oblique angle of incidence; it can also occur when the ratio $\alpha = a_{1y}/a_{1x}$ is accidentally close to

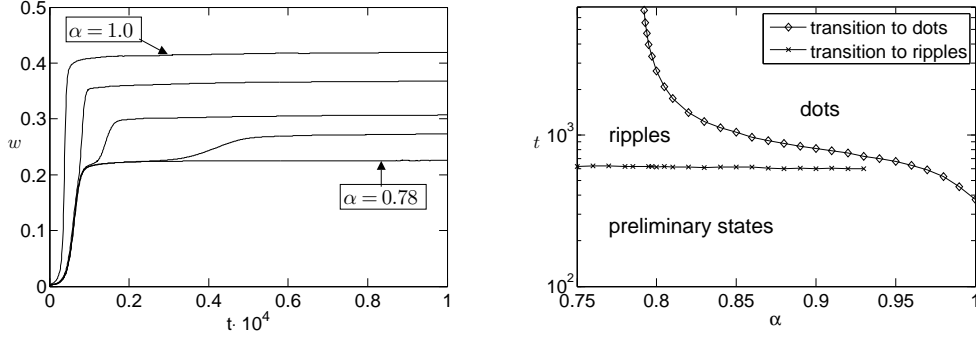


FIG. 3: Left panel: Temporal evolution of the surface roughness w . for $\gamma = 0.24$, $\beta = 2.0$, $\alpha = 1.0, 0.9, 0.82, 0.795, 0.78$ corresponding to the curves from top to bottom using an ensemble average over 40 runs. Right panel: Transition time t_c to ripples and dots as function of α with fixed parameters $\gamma = 0.24$ and $\beta = 2.0$. The regions where dots or ripples exist are delimited by the turning points of the surface roughness $w(t)$ as indicated in the left panel. For $\alpha > 0.93$ only one turning point can be distinguished.

unity for more oblique angles of incidence and, consequently, also hexagonally ordered dot structures show up in such parameter ranges. So far, the transition from ripples to dots, α_T has been obtained for a fixed value of γ . Numerical tests indicate that the transition line $\alpha_T(\gamma)$ merges into the linear instability $\gamma = 0.25$ as $\alpha \rightarrow 1$. Finally, as a result of the afore-mentioned property (A) of (4), an analogous scenario happens close the instability of $h_{FF} = 0$ for $\alpha > 0$ with the roles of n- and t-ripples being exchanged.

Effect of damping. - To understand the role of the non-local term in (1) or the damping in (4), respectively, we show as a representative example in the first panel from the left of Fig.4 late stages of the surface morphology for the same values as in the third row of Fig. 2, except that the damping parameter has been drastically reduced to a value of $\gamma = 0.06$. Obviously, lowering γ has the effect that the rather periodic hexagonal dot structure seen for $\gamma = 0.24$ has been coarsened into a pattern consisting of irregularly sized, droplet-like structures with a preferential elongation in y -direction. Flipping the sign of α for this parameter constellation, as shown in the second and third panel of Fig. 4, the initial and late stages of the surface evolution exhibit strong, irregular superimposed modulations of the n-ripples in the y -direction. Consequently, the damping γ acts as a order-disorder parameter, i.e. it gradually changes the pattern from the maximally disordered limit for $\gamma = 0$, i.e. the aKSE limit, to a quite regular ripple or dot pattern close to $\gamma = 0.25$ (if

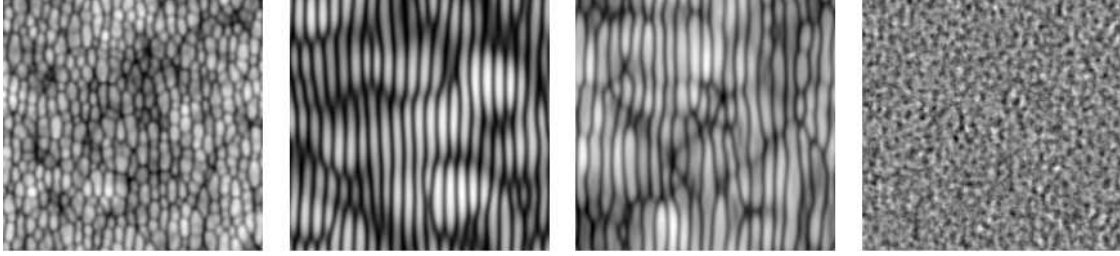


FIG. 4: Influence of the damping γ on the surface morphology. From left to right: low damping $\gamma = 0.06$ for a late stage ($t = 10^4$) at $\alpha = 0.8$, $\beta = 2.0$, an early stage ($t = 50$) at $\alpha = -0.8$, $\beta = 2.0$, and corresponding late stage ($t = 10^4$); strong damping $\gamma = 0.3$ for a late stage ($t = 10^4$) at $\alpha = 0.8$, $\beta = 2.0$. Surface roughness for these four parameter constellations averaged over 40 runs, left to right: $w = 1.25, 1.02, 1.16, 1.79 \cdot 10^{-3}$.

$\alpha < 1$). For even larger γ , the deterministic limit of the adKSE possesses a linearly stable flat surface. Due to the nonzero stochasticity η in our simulations, however, the resulting pattern for such values of γ is stochastically rough, as depicted in the fourth panel of Fig.4. Most remarkably, the corresponding surface roughness is drastically reduced (by almost three orders of magnitude) in comparison to the cases with $\gamma \leq 0.24$. Therefore, the pattern for $\gamma > 1/4$, can be interpreted as a basically smooth surface with some stochastic variations that reflect the stochastic component of the sputter process. Such patterns have recently been reported by Frost et al. [17]. As a consequence, transitions to such basically smooth patterns triggered by changing the angle of incidence are precluded by a quite regular ripple or dot pattern. Assuming a nonlinear dependence of α and γ on the angle of incidence and keeping β fixed (cf. also Fig.1), a variety of distinct transitions between patterns such as n-ripples \leftrightarrow smooth surfaces \leftrightarrow t- or n-ripples, n-ripples \leftrightarrow dot structures \leftrightarrow t- or n-ripples as well as more disordered states seem to be possible. Some of these transitions have been experimentally reported in [6, 7, 8] (cf. also our introductory part). Using property (B) of Eq. (3), we also infer that patterns that look like negative images (e.g. mounds exchanged by holes) of the ones in Fig.4 can be seen by going to negative values of a_{3x} and a_{3y} . Finally, our numerical simulations show that the transition to hexagonally arranged dots is generically subcritical implying that starting from an appropriately prestructured surface, dot patterns might evolve even for $\gamma > 1/4$.

Cancellation modes (CM). - Straight ripples oriented obliquely to the x -direction, as

found by Rost and Krug [10] in the aKSE, can also be recovered in the adKSE. Assuming solutions $h(x, y, t) = f(x - uy, t)$ that are constant along lines $x = s + uy$ and demanding that the nonlinearity in the adKSE vanishes, implies $u = \pm\sqrt{-1/\beta}$. Their evolution governed by $\partial_t f = -(\gamma + 1 + \alpha u^2)\partial_s^2 f - (1 + u^2)^2\partial_s^4 f$ has the maximum growth rate $\sigma_{max} = -\gamma + (\beta - \alpha)^2/[4(1 - \beta)^2]$ at a wave number $q = \sqrt{\beta(\beta - \alpha)/2(\beta - 1)^2}$. Consequently, CM exist only if $\beta < 0$ and $\alpha > \beta$ as in the case of the aKSE [10]. Remarkably, CM exist as stationary solutions if $\gamma = (\beta - \alpha)^2/[4(1 - \beta)^2]$ in contrast to the aKSE [10].

Conclusions. - The adKSE (4) presented here seems to be a promising candidate for a continuum model for low energy ion-beam erosion under oblique ion incidence since it can reproduce many distinct types of patterns also seen in experiments. To substantiate this, comparison with so far not available detailed experimental studies is needed. A more detailed discussion of the deterministic adKSE focussing on the bifurcation structure of its patterns will be given elsewhere [18].

-
- [1] NAVEZ M., SELLA C., AND CHAPEROT D., *Compt. Rend.* **254** (1962) 240
 - [2] CARTER G., *J. Phys. D: Appl. Phys.* **34** (2001) R1; VALBUSA U., BORAGNO C., AND BUATIER DE MONGEOT F., *J. Phys.: Condens. Matter* **14** (2002) 8153.
 - [3] MAKEEV M.A., CUERNO R., AND BARABÁSI A.-L., *Nucl. Instr. and Meth. B* **197** (2002) 185
 - [4] FACSKO S., DEKORSY T., KOERDT C., TRAPPE C., KURZ H., VOGT A. AND HARTNAGEL H., *Science* **285** (1999) 1551; FACSKO S., AND KURZ H., DEKORSY T., *Phys. Rev. B* **63** (2001) 165329.
 - [5] FROST F., SCHINDLER A., AND BIGL F., *Phys. Rev. Lett.* **85** (2000) 4116; FROST F. AND RAUSCHENBACH B., *Appl. Phys. A* **77** (2003) 1; FROST F., ZIBERI B., HÖCHE T., AND RAUSCHENBACH B., *Nucl. Instr. and Meth. B* **216** (2004) 9.
 - [6] ZIBERI B., FROST F., HÖCHE T., AND RAUSCHENBACH B., *Phys. Rev. B* **72** (2005) 235310.
 - [7] ZIBERI B., FROST F., AND RAUSCHENBACH B., *Formation of large-area nanostructures on Si and Ge surfaces during low-energy ion beam erosion*, *J. Vac. Sci. Technol. A* **24**, July/August issue 2006.
 - [8] ALLMERS T, DONATH M, AND RANGELOV G., *J. Vac. Sci. Technol. B* **24** (2006) 582.

- [9] CUERNO R. AND BARABÁSI A.-L., *Phys. Rev. Lett.* **74** (1995)4746; PARK S., KAHNG B., JEONG H. AND BARABÁSI A.-L., *Phys. Rev. Lett.* **83** (1999) 3486.
- [10] ROST M. AND KRUG J., *Phys. Rev. Lett.* **75** (1995) 3894.
- [11] BRADLEY R.M. AND HARPER J.M.E., *J. Vac. Sci. Technol. A* **6** (1988) 2390.
- [12] KIM T.C. et al. , *Phys. Rev. Lett.* **92** (2004) 246104 (2004).
- [13] CASTRO M., CUERNO R., VÁZQUEZ L. AND GAGO R., *Phys. Rev. Lett.* **94**, (2005) 016102.
- [14] RAIBLE M., LINZ S.J., AND HÄNGGI P., *Phys. Rev. E* **62** (2000) 1691; *Phys. Rev. E* **64** (2001) 031506.
- [15] FACSKO S., BOBEK T., STAHL A., KURZ H., AND DEKORSY T., *Phys. Rev. B* **69** (2004) 153412.
- [16] VOGEL S. AND LINZ S.J., *Phys. Rev. B* **72** (2005) 035416.
- [17] FROST F., FECHNER R., FLAMM D., ZIBERI B., FRANK W. AND RAUSCHENBACH B., *Appl. Phys A* **78** (2004) 651.
- [18] REHWALD C, DREIMANN C., VOGEL S. AND LINZ S.J., *Bifurcation behavior of the damped anisotropic Kuramoto-Sivashinsky equation*, in preparation.